

The third instrument collected whole air samples in evacuated 2-l electropolished stainless-steel canisters. The canisters were pressurized to 40 p.s.i., and then shortly after each flight were transported to a central laboratory. A 1,520-ml air sample was cryogenically trapped on a loop filled with glass beads maintained at liquid nitrogen temperature. Multi-column gas chromatography coupled with flame ionization detection and mass spectrometry was used to quantify C₂–C₈ NMHCs (alkanes, alkynes, alkenes and aromatics). Sample analysis usually occurred within one week of collection and never more than two weeks. The overall accuracy of these NMHC measurements is estimated to be 5–10%. The limit of detection was 3 p.p.t. for all NMHCs²⁷. Additional details may be obtained from the authors.

Received 22 August 2000; accepted 20 February 2001.

1. Singh, H. B., Kanakidou, M., Crutzen, P. & Jacob, D. High concentrations and photochemical fate of carbonyls and alcohols in the global troposphere. *Nature* **378**, 50–54 (1995).
2. Wennberg, P. O. *et al.* Hydrogen radicals, nitrogen radicals, and the production of ozone in the upper troposphere. *Science* **279**, 49–53 (1998).
3. Carlier, P., Hannachi, H. & Mouvrier, G. The chemistry of carbonyls in the atmosphere—a review. *Atmos. Environ.* **20**, 2079–2099 (1986).
4. Prather, M. & Jacob, D. A persistence imbalance in HO_x and NO_x photochemistry of the upper troposphere driven by deep tropical convection. *Geophys. Res. Lett.* **24**, 3189–3192 (1997).
5. Müller, J. F. & Brasseur, G. Sources of upper tropospheric HO_x: A three-dimensional model study. *J. Geophys. Res.* **104**, 1705–1715 (1999).
6. Jaeglé, L., Jacob, D., Brune, W. & Wennberg, P. Chemistry of HO_x radicals in the upper troposphere. *Atmos. Environ.* **35**, 469–489 (2001).
7. Murphy, D. M., Thomson, D. S. & Mahoney, M. J. *In situ* measurements of organics, meteoritic material, mercury, and other elements in aerosols at 5 to 19 kilometers. *Science* **282**, 1664–1669 (1998).
8. Li, P. *et al.* Heterogeneous reactions of VOCs on oxide particles of the most abundant crustal elements: surface reactions of acetaldehyde, acetone and propionaldehyde on SiO₂, Fe₂O₃, TiO₂ and CaO. *J. Geophys. Res.* (in the press).
9. Raper, J. L. *et al.* Pacific Exploratory Mission in the tropical pacific: PEM-Tropics B, March–April 1999. *J. Geophys. Res.* (in the press).
10. Atlas, E. *et al.* Alkyl nitrate and selected halocarbon measurements at Mauna Loa observatory, Hawaii. *J. Geophys. Res.* **97**, 10331–10348 (1992).
11. Singh, H. B. & Hanst, P. L. Peroxyacetyl nitrate (PAN) in the unpolluted atmosphere: An important reservoir for nitrogen oxides. *Geophys. Res. Lett.* **8**, 941–944 (1981).
12. Arlander, D. W., Brunking, D., Schmidt, U. & Ehhalt, D. H. The distribution of acetaldehyde in the lower troposphere during TROPOZ II. *J. Atmos. Chem.* **22**, 243–249 (1995).
13. Riemer, D. *et al.* Observations of nonmethane hydrocarbons and oxygenated volatile organic compounds at a rural site in the southeastern United States. *J. Geophys. Res.* **103**, 28111–28128 (1998).
14. Lamanna, M. S. & Goldstein, A. H. *In situ* measurements of C₂–C₁₀ VOCs above a Sierra-Nevada pine plantation (including oxygenated species) from pasture. *J. Geophys. Res.* **104**, 21247–21262 (1999).
15. Singh, H. B. *et al.* Distribution and fate of selected oxygenated organic species in the troposphere and lower stratosphere over the Atlantic. *J. Geophys. Res.* **105**, 3795–3805 (2000).
16. Singh, H. B. & Zimmerman, P. B. in *Advances in Environmental Science and Technology* Vol. 24 (ed. Nariagu, J.) 177–235 (Wiley and Sons, New York, 1992).
17. Staudt, A. C. *et al.* Continental sources, transoceanic transport, and interhemispheric exchange of carbon monoxide over the Pacific. *J. Geophys. Res.* (submitted); preprint at (<http://www-as.harvard.edu/chemistry/trop>) (2001).
18. Logan, J. *et al.* Tropospheric chemistry: A global perspective. *J. Geophys. Res.* **86**, 7210–7254 (1981).
19. Kesselmeier, J. & Staudt, M. Biogenic volatile organic compounds (VOC): An overview on emissions, physiology and ecology. *J. Atmos. Chem.* **33**, 23–38 (1999).
20. Madronich, S. & Calvert, J. G. Permutation reactions of organic peroxy radicals in the troposphere. *J. Geophys. Res.* **95**, 5697–5715 (1990).
21. Reissell, A. *et al.* Formation of acetone from the OH radical- and O₃-initiated reactions of a series of monoterpenes. *J. Geophys. Res.* **104**, 13869–13879 (1999).
22. Crutzen, P. J. *et al.* High spatial and temporal resolution measurements of primary organics and their oxidation products over the tropical forests of Surinam. *Atmos. Environ.* **34**, 1161–1165 (2000).
23. Nemecek-Marshall, M. *et al.* Marine *Vibrio* species produce the volatile organic compound acetone. *Appl. Environ. Microbiol.* **61**, 44–47 (1995).
24. Zhou, X. & Mopper, K. Photochemical production of low-molecular-weight carbonyl compounds in seawater and surface microlayer and their air-sea exchange. *Mar. Chem.* **56**, 201–213 (1997).
25. Lee, M., Noone, B. C., O’Sullivan, D. & Heikes, B. G. Method for the collection and HPLC analysis of hydrogen peroxide and C₁ and C₂ hydroperoxides in the atmosphere. *J. Atmos. Ocean Technol.* **12**, 1060–1070 (1995).
26. Lazrus, A. L., Fong, K. L. & Lind, J. A. Automated fluorometric determination of formaldehyde in air. *Anal. Chem.* **60**, 1074–1078 (1988).
27. Blake, N. J. *et al.* Influence of southern hemispheric biomass burning on mid-tropospheric distributions of nonmethane hydrocarbons and selected halocarbons over the remote South Pacific. *J. Geophys. Res.* **104**, 16213–16232 (1999).

Acknowledgements

This research was supported by the NASA Global Tropospheric Experiment. We thank all participants in NASA/PEM-Tropics B for their support.

Correspondence and requests for materials should be addressed to H.S. (e-mail: hsingh@mail.arc.nasa.gov).

Hemispherical variations in seismic velocity at the top of the Earth’s inner core

Fenglin Niu* & Lianxing Wen†

* Department of Terrestrial Magnetism, Carnegie Institution of Washington, 5241 Broad Branch Road NW, Washington DC 20015, USA

† Department of Geosciences, State University of New York at Stony Brook, Stony Brook, New York 11794, USA

Knowledge of the seismic velocity structure at the top of the Earth’s inner core is important for deciphering the physical processes responsible for inner-core growth^{1–3}. Previous global seismic studies^{4–9} have focused on structures found 100 km or deeper within the inner core, with results for the uppermost 100 km available for only isolated regions^{10–12}. Here we present constraints on seismic velocity variations just beneath the inner-core boundary, determined from the difference in travel time between waves reflected at the inner-core boundary and those transmitted through the inner core. We found that these travel-time residuals—observed on both global seismograph stations and several regional seismic networks—are systematically larger, by about 0.8 s, for waves that sample the ‘eastern hemisphere’ of the inner core (40° E to 180° E) compared to those that sample the ‘western hemisphere’ (180° W to 40° E). These residuals show no correlation with the angle at which the waves traverse the inner core; this indicates that seismic anisotropy is not strong in this region and that the isotropic seismic velocity of the eastern hemisphere is about 0.8% higher than that of the western hemisphere.

PKiKP is the P wave that reflects off the inner-core boundary (ICB) and PKIKP is the P wave that propagates through the inner core. The differential travel time between these two phases is most sensitive to the seismic structure in the inner core, as these two phases have almost identical ray paths in the mantle at the distance range of 130°–142° (Fig. 1 inset). At this distance range, PKiKP samples the top 100 km of the inner core, and both PKiKP and PKIKP are identifiable in short-period seismograms. We select a total of 203 high-quality PKiKP and PKIKP waveforms from recordings in the IRIS global seismic network (GSN) and many regional seismic arrays. We choose recordings for events from 1990 to 1999 with simple source–time functions, so only those of intermediate and deep earthquakes are used. Broadband seismograms are filtered using the WWSSN short-period instrument response.

Differential travel-time residuals of PKiKP – PKIKP show a clear difference between the ‘eastern hemisphere’ and the ‘western hemisphere’ of the inner core (Fig. 1). A positive (negative) travel-time residual indicates a relatively higher (lower) seismic velocity in the top of the inner core compared to the PREM model¹³. The travel-time residuals are systematically larger in the eastern hemisphere (solid symbols) than those in the western hemisphere (open symbols), regardless of the turning depths of the PKiKP phases (Fig. 2a). These travel-time residuals, on the other hand, show no correlation with the PKiKP ray angles from the equatorial plane (Fig. 2b), indicating that anisotropy is non-existent or very weak in the outermost 100 km of the inner core. This is consistent with the travel-time and waveform studies using regional data^{10–12}. On average, the residuals in the eastern hemisphere are approximately 0.8 s larger than those of the western hemisphere. The travel-time residuals observed in the eastern hemisphere can be fitted by a model with P velocities that are roughly 0.5% faster than the PREM in the top 100 km of the inner core, whereas those observed in the

western hemisphere can be explained by a model with P velocities that are 0.3% slower than the PREM (Fig. 2a). Further precise models using waveform data are presented in elsewhere¹⁴.

We only used those seismograms that have unambiguous PKiKP and PKIKP phases and clear move-outs (arrival times as a function of epicentral distance) of these two phases. The move-outs of these two phases are clear from the compilations of all observed waveforms in both hemispheres. We show an example of these move-outs of the PKiKP and PKIKP phases from record sections observed in two regional seismic arrays (Fig. 3a and b). In practice, because the onsets in the worldwide standardized seismograph network

(WWSSN) responses are sometimes difficult to identify, we determine the differential travel time between PKiKP and PKIKP phases by measuring the relative timing between their maximal amplitudes. The above picking method has been shown to be very accurate in synthetic seismograms at the distance range between 130° and 141° (Fig. 3c). These synthetics are calculated by the generalized ray theory¹⁵ using the PREM model and a source depth of 600 km. With respect to the maximal amplitudes of the PKiKP phases, the hand-picked PKIKP times based on their maximal amplitudes (vertical lines) and those calculated (dots) are in good agreement. The difference is less than 0.06 s. This difference is

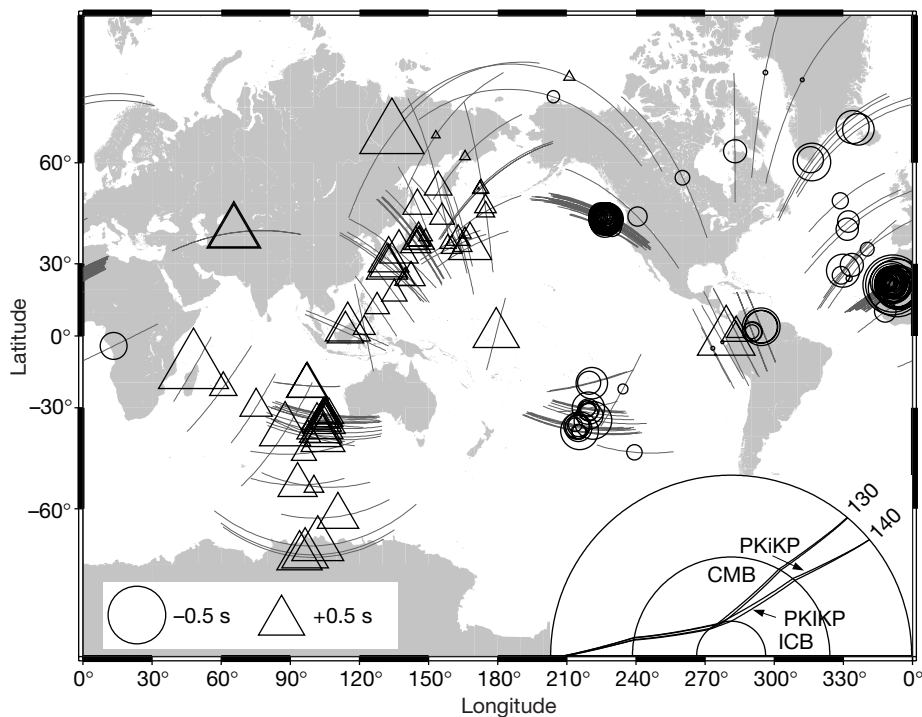


Figure 1 Map view of PKiKP minus PKIKP travel-time residuals displayed as lines along ray segments through the inner core and symbols at the turning points. The residuals are calculated with respect to the PREM. Circles and triangles represent negative and positive residuals, respectively. The size of the symbols is proportional to the absolute value of residuals. The data set was collected from the global seismic network (GSN) and many

regional seismic networks: (1) the J-array¹⁷; (2) the Canadian national seismograph network (CNSN); (3) the Tanzania broadband seismic experiment; (4) The broadband Andean joint experiment (BANJO); (5) the BLSF 94; (6) the Tibetan Plateau passive-source seismic experiment (TIPLT). Ray paths of PKiKP and PKIKP at distances 130° and 140° are shown in the inset.

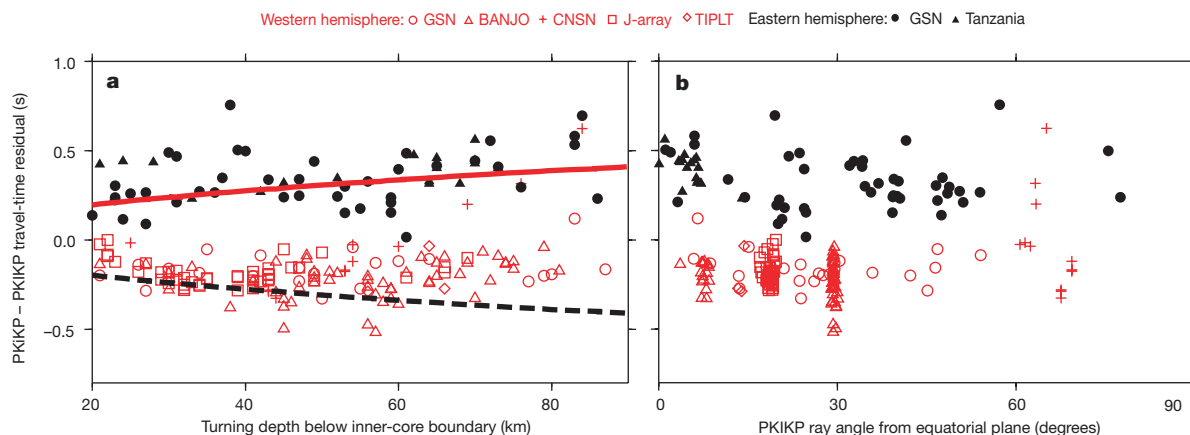


Figure 2 PKiKP – PKIKP travel-time residuals as a function of turning depth and angle. Residuals as function of (a) PKiKP turning depth below the ICB and (b) PKiKP ray angle from the equatorial plane. Solid and open symbols represent the eastern and western

hemispheres, respectively. The predicted PKiKP – PKIKP travel-time residuals for two models with a top 100-km layer 0.5% faster (solid line) and 0.5% slower (dotted line) than the PREM in the inner core are shown.

almost the same as the data-sampling rate and is much less than the observed time difference between the two hemispheres. The uncertainty in picking the maximal amplitudes is ± 0.10 s. We have excluded the data in the distances that are less than 130° , because PKiKP and PKiKP waveforms interfere with each other in this distance range.

The observed hemispherical distribution of PKiKP – PKiKP

travel-time residual cannot be explained by variation of the inner-core radius. An increase or decrease of the inner-core radius at the piercing points of PKiKP rays and the reflection points of PKiKP rays (Fig. 1 inset) would have almost no effect on PKiKP – PKiKP time. Small-scale topography, which may affect these two phases differently, is also an unlikely explanation for our observation, because the piercing points of PKiKP rays and the reflection

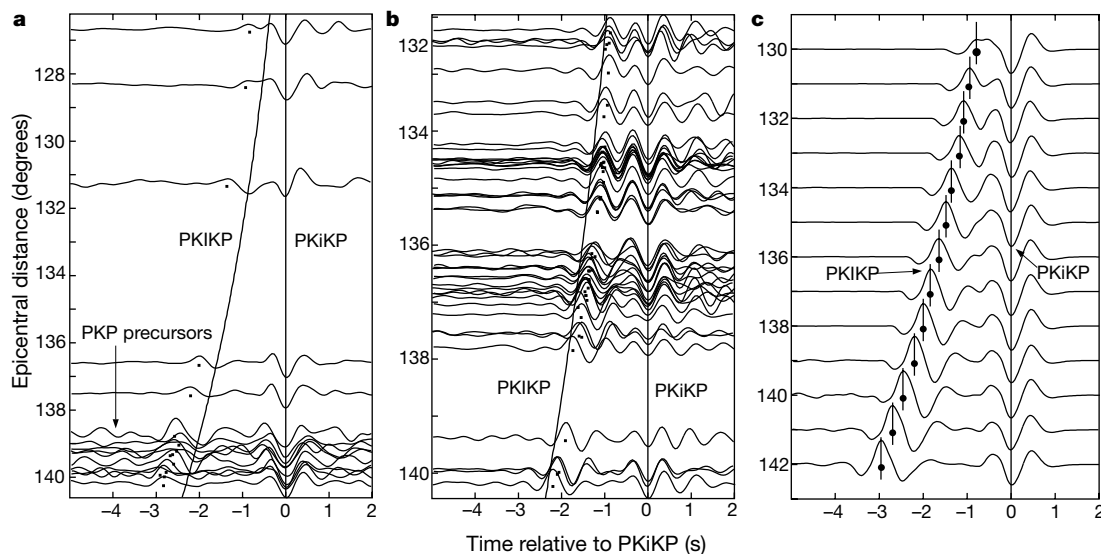


Figure 3 Examples of seismograms. Experimental seismograms were recorded in the Tanzania array (a) and the J-array (b), and synthetic seismograms were calculated by the generalized ray theory (c). All the seismograms are aligned according to the PKiKP arrivals. Observed and PREM¹³ travel times of PKiKP are indicated by dots and straight

line, respectively. a, 18 December 1994 at a source depth of 551.0 km and with $M_w = 5.7$. b, 26 April 1999 at a source depth of 174.0 km with $M_w = 5.9$. c, PKiKP resulted from waveform handpicking and ray tracing are indicated by vertical lines and dots, respectively.

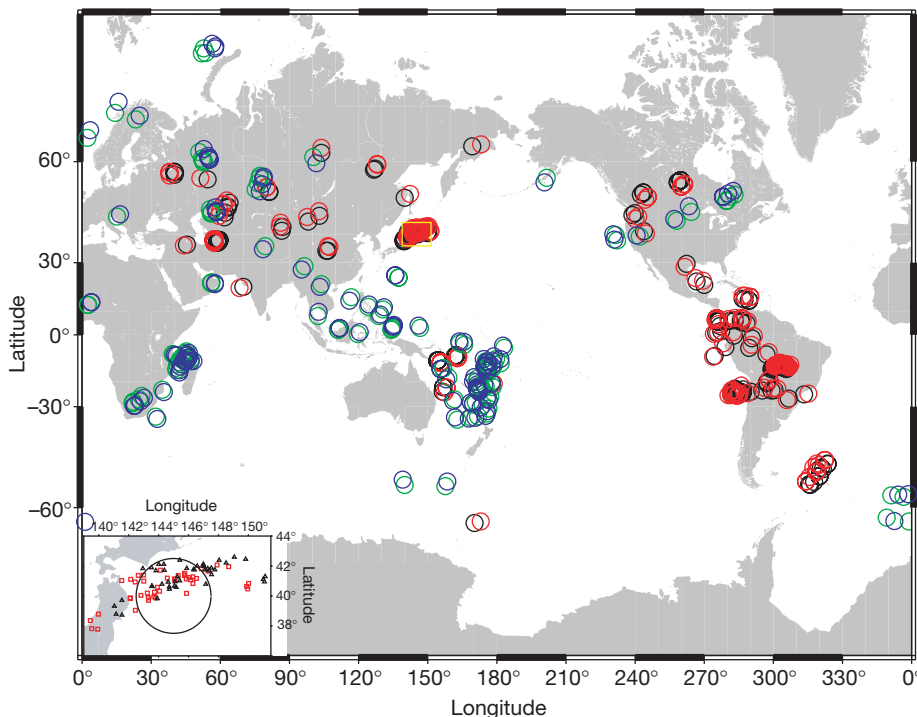


Figure 4 Distribution of hit points of PKiKP and PKiKP rays at the CMB. Black and red circles represent those of PKiKP and PKiKP bouncing at the western hemisphere of the top of the inner core; blue and green circles are those bounding at the eastern hemisphere. The size of the circles is roughly equal to the Fresnel zone of PKiKP and PKiKP at the CMB

for a 1-Hz wave. The hit points within the yellow rectangle region, which are core exits of PKiKP and PKiKP observed by the J-array for the event 04/26/99, are shown in the inset. They are indicated by squares for PKiKP and triangles for PKiKP. A circle with a radius of 150 km is shown to indicate roughly the size of the Fresnel zone.

points of PKiKP rays at the ICB overlap in some regions (such as the western Pacific Ocean).

The systematic variation of these differential travel times is also unlikely to be explained by the heterogeneities near the core–mantle boundary (CMB). In Fig. 4, we plot the hit points of PKiKP and PKiKP at the CMB using different colours, with black (PKiKP) and red (PKiKP) circles centring their bounding points in the western hemisphere and blue (PKiKP) and green (PKiKP) circles in the eastern hemisphere. The size of the circle is the same as the Fresnel zone of PKiKP and PKiKP at the CMB. The Fresnel zone is approximately 150 km at the CMB for a vertically propagating, short-period (about 1 Hz) P-wave. The separation between the PKiKP and PKiKP paths is, however, only about 50 km at the CMB. Because their Fresnel zones overlap (black and red circles; blue and green circles), the heterogeneities near the CMB would affect both phases in the same way. Thus the heterogeneities at the CMB would have little effect on the differential travel time of these two phases. Furthermore, some regions of the CMB (for example, Tonga, Europe; Fig. 4) are sampled by both rays bottoming in different hemispheres. In regions covered by dense seismic arrays, the PKiKP and PKiKP hit points overlap even for different observations. Detailed distribution of the hit points of PKiKP (red squares) and PKiKP (black triangles) observed by the dense J-array for the event on 26 April 1999 is shown in the inset of Fig. 4. The PKiKP – PKiKP travel-time residuals thus can only be attributed to the heterogeneity within the inner core.

In general, global PKiKP – PKiKP residual times are less scattered than PKP – PKiKP data, indicating that they are less biased by the seismic structures near the CMB and that our argument is reasonable. Our results are in good agreement with a PKP – PKiKP travel-time residual study⁸, which first suggested a degree-one longitudinal distribution of heterogeneity in the top 100–500 km of the inner core. The PKP – PKiKP travel-time residuals are also affected by the structure of the uppermost 100 km of the inner core. Preliminary calculations suggest that our models can explain most of the PKP – PKiKP travel-time residuals.

The hemispherical distribution of heterogeneity in the top 100 km of the inner core may reflect some features of the inner-core growth. It may be caused either by an intrinsic difference during inner-core formation, or an external temperature difference at the base of the outer core. However, the former mechanism seems unlikely when we consider that the top 100 km of the inner core, as observed here, is clearly different from the rest of the inner core; the core structure is characterized by an axisymmetric anisotropic structure with a north–south fast axis^{4–7}. Seismic velocity in the outermost inner core may be related to the temperature at the bottom of the liquid outer core, because the temperature will control the freezing rate of the liquid iron and therefore affects the seismic velocity of the solid iron. A recent experimental study¹⁶ suggests that a cold downwelling at the CMB may generate a hemispherical variation of temperature above the ICB. The problems are whether and for how long the heterogeneity at the CMB can simply be represented by a higher-velocity region in the western Pacific. Therefore, the implication of the presence of a different layer in the outermost region of the inner core is very important to our understanding of the physical process of inner-core growth, and also of mantle dynamics. □

Received 18 July 2000; accepted 28 February 2001.

- Yoshida, S., Sumita, I. & Kumazawa, M. Growth model of inner core coupled with the outer core dynamics and resulting elastic anisotropy. *J. Geophys. Res.* **101**, 28085–28103 (1996).
- Anderson, O. L. Mineral physics of iron and of the core. *Rev. Geophys.* **33**, 429–441 (1995).
- Boehler, R. Temperatures in the Earth's core from melting point measurements of iron at high static pressure. *Nature* **363**, 534–536 (1993).
- Morelli, A., Dziewonski, A. M. & Woodhouse, J. H. Anisotropy of the core inferred from PKiKP travel times. *Geophys. Res. Lett.* **13**, 1545–1548 (1986).
- Shearer, P. M., Toy, K. M. & Orcutt, J. A. Axi-symmetric Earth models and inner-core anisotropy. *Nature* **333**, 228–232 (1988).

- Creager, K. C. Anisotropy of the inner core from differential travel times of the phases PKP and PKiKP. *Nature* **356**, 309–314 (1992).
- Tromp, J. Support for anisotropy of the Earth's inner core from oscillations. *Nature* **366**, 678–681 (1993).
- Tanaka, S. & Hamaguchi, H. Degree one heterogeneity and hemispherical variation of anisotropy in the inner core from PKP(BC) – PKP(DF) times. *J. Geophys. Res.* **102**, 2925–2938 (1997).
- Creager, K. C. Large-scale variations in inner core anisotropy. *J. Geophys. Res.* **104**, 23127–23139 (1999).
- Cormier, V. F. & Choy, G. L. A search for lateral heterogeneity in the inner core from differential travel times near PKP-D and PKP-C. *Geophys. Res. Lett.* **13**, 1553–1556 (1986).
- Song, X. & Helmberger, D. V. Depth dependence of anisotropy of the Earth's inner core. *J. Geophys. Res.* **100**, 9805–9816 (1995).
- Kaneshima, S. Mapping heterogeneity of the uppermost inner core using two pairs of core phases. *Geophys. Res. Lett.* **23**, 3075–3078 (1996).
- Dziewonski, A. M. & Anderson, D. L. Preliminary reference Earth model. *Phys. Earth Planet. Int.* **25**, 297–356 (1981).
- Wen, L. & Niu, F. Seismic velocity and attenuation structures in the top of the Earth's inner core. *J. Geophys. Res.* (submitted).
- Helmberger, D. V. in *Earthquakes: Observation, Theory and Interpretation* (ed. Kanomori, H.) 173–222 (Soc. Italiana Di Fisica, Bologna, 1983).
- Sumita, I. & Olson, P. A laboratory model for convection in Earth's core driven by a thermally heterogeneous mantle. *Science* **286**, 1547–1549 (1999).
- J-Array Group. The J-Array program: system and present status. *J. Geomag. Geoelectr.* **45**, 1265–1274 (1993).

Acknowledgements

We are grateful to the IRIS, J-array Data Center, W. Shannon and L. Saumure for supplying the data. We thank S. Tanaka for providing us their PKP-PKiKP data. We also thank H. Kawakatsu, S. Sacks and P. Silver for comments on the manuscript. Discussions with J. Aurnou, M. Fouch, W. Holt, S. Solomon, I. Sumita, S. Tanaka and D. Weidner were helpful in preparing the manuscript. This work is supported by the fellowship of the Carnegie Institution of Washington and an NSF grant.

Correspondence and requests for materials should be addressed to F.N. (e-mail: niu@dtm.ciw.edu).

The distribution of integumentary structures in a feathered dinosaur

Qiang Ji*, Mark A. Norell†, Ke-Qin Gao†, Shu-An Ji* & Dong Ren*

*Chinese Academy of Geological Sciences, 26 Baiwanzhuang, Beijing 100037, People's Republic of China

†American Museum of Natural History, Central Park West at 79th Street, New York, New York 10024-5192, USA

Non-avian theropod dinosaurs with preserved integumentary coverings are becoming more common^{1–6}; but apart from the multiple specimens of *Caudipteryx*, which have true feathers^{2,7}, animals that are reasonably complete and entirely articulated that show these structures in relation to the body have not been reported. Here we report on an enigmatic small theropod dinosaur that is covered with filamentous feather-like structures over its entire body.

The new specimen was collected from the extensive deposits of the Yixian Formation at Lingyuan, Liaoning, China. These fossil beds have produced many fossil specimens with preserved soft body structures^{8–12}. Notable among these are fossil bird specimens^{9,10}. Although some specimens from western Liaoning have been shown to be composites¹³ or forgeries¹⁴, the integrity of the specimen described here is assured because both slabs match up exactly and the integumentary covering lies below flakes of rock in several places: it is therefore not painted, scratched into the matrix or otherwise enhanced.

Theropoda Marsh 1881
Coelurosauria Huene 1914
Maniraptora Gauthier 1986
Dromaeosauridae Matthew & Brown 1922
Gen. et sp. indet.